Bis(Naphthalene Imide)diphenylanthrazolines: A New Class of Electron Acceptors for Efficient Nonfullerene Organic Solar Cells and Applicable to Multiple Donor Polymers

ARTICLE *in* ADVANCED ENERGY MATERIALS · APRIL 2015

Impact Factor: 16.15 · DOI: 10.1002/aenm.201402041

4 AUTHORS, INCLUDING:

Taeshik Earmme
University of Washington Seattle
18 PUBLICATIONS **491** CITATIONS
SEE PROFILE

Selvam Subramaniyan
University of Washington Seattle
33 PUBLICATIONS **860** CITATIONS
SEE PROFILE

Bis(Naphthalene Imide)diphenylanthrazolines: A New Class of Electron Acceptors for Efficient Nonfullerene Organic Solar Cells and Applicable to Multiple Donor Polymers

*Haiyan Li, Taeshik Earmme, Selvam Subramaniyan, and Samson A. Jenekhe**

Unlike universally applicable fullerene derivatives, current nonfullerene electron acceptors are rarely effective with more than one donor polymer in bulk heterojunction (BHJ) solar cells. A novel class of nonfullerene electron acceptors, bis(naphthalene imide)-3,6-diphenyl-*trans*-anthrazolines (BNIDPAs), that is applicable and yields efficient photovoltaic devices with multiple donor polymers, including a thiazolothiazole–dithienosilole copolymer (PSEHTT) and benzodithiophene copolymers (PBDTT-FTTE and PTB7) is reported. Photovoltaic devices composed of the BNIDPA-butyloctyl (BO) acceptor with PSEHTT, PBDTT-FTTE, and PTB7, respectively, have power conversion efficiencies of 3.0%–3.1% with high open-circuit voltages of ≈1.0 V. In contrast, BHJ devices composed of BNIDPA-DT acceptor with larger 2-decyltetradecyl chains and the same donor polymers have substantially reduced bulk electron mobility and reduced photovoltaic efficiencies of 1.3%–1.7%, which highlight the critical role of the size of alkyl chains appended onto nonfullerene electron acceptors. The present results provide a rare example of nonfullerene electron acceptors that are capable of pairing with multiple donor polymers to achieve efficient BHJ solar cells.

1. Introduction

Increasing efforts have recently been devoted to fullerene-free organic photovoltaics (OPVs) because of their potential to overcome the drawbacks of fullerene-based devices (e.g., poor photostability in air, poor solar energy harvesting by the fullerene acceptors, low photovoltages, etc).[1–7] Both small molecules[8–37] and polymers[38–48] are being explored as alternative electron-acceptor materials. Small-molecule nonfullerene electron acceptors[8–37] are of particular interest because (i) strong absorption in the visible and near-infrared region and/or relatively high lowest unoccupied molecular orbital (LUMO) energy level that is higher lying compared with fullerene derivatives can be readily realized for achieving a high photovoltage while maintaining efficient solar light harvesting; (ii) small-molecule materials of high purity can be achieved by routine purification techniques with no batch-to-batch variation in quality; and (iii) unlike fullerene derivatives whose backbones are limited to very few all-carbon clusters (e.g., C_{60}, C_{70}, and C_{80}) that undergo limited reactions, a variety of nonfullerene molecular building blocks are available through versatile synthetic organic chemistry.[8–37] The design and synthesis of new nonfullerene acceptors could potentially offer opportunities for tuning the electronic structure, light harvesting properties, crystallinity, charge transport, and compatibility with donor polymers to further improve the efficiency, stability, and scalability of OPVs.

Nonfullerene electron acceptors of various molecular structures have been explored, including simple monochromophoric molecules,[11–15,18,19,24,26,34] linear dichromophoric,[20,21,28,31–33,35–37] trichromophoric,[10,25,27] and star-shape oligomers[17,22,23] and polymers.[38–48] Among these, naphthalene diimide (NDI) and perylene diimide (PDI) small molecules and polymers have been extensively investigated, leading to recent demonstration of nonfullerene bulk heterojunction (BHJ) devices with power conversion efficiencies (PCEs) of up to 3%–6%[15–24,31,33,34,39–41,43,46–48] Other nonfullerene acceptors with promising PCEs of 2%–4% include: benzothiadiazole,[25,27] phthalimide,[25,27] diketopyrrolopyrrole,[17,38] indan-1,3-dione,[28] fluoroanthene imide,[13,14] azadipyrromethene-based Zn(II) complexes,[29] and dicyanodistyrylbenzene-naphthaleneimide.[30] However, unlike the ubiquitous fullerene-type electron acceptors, such as [6,6]-phenyl-C_{60}-butyric acid methyl ester ($PC_{60}BM$) and [6,6]-phenyl-C_{70}-butyric acid methyl ester ($PC_{70}BM$) that work efficiently with many donor polymers, i.e. are universally applicable, current nonfullerene acceptors have generally been reported to be effective with one donor polymer and rarely with two or more donor polymers.[23,33] The development of new electron acceptors that are applicable to multiple donor polymers in BHJ solar cells is thus highly desired toward the realization of high performance fullerene-free OPVs.

Diphenylanthrazoline (DPA) represents an important electron-accepting building block that was previously used to design various small-molecule and polymeric semiconductors.[49–53] Previous studies showed that arylene substituted DPA small molecules[50] and ladder-type bisindenoanthrazolines[49] could be used as effective electron-transporting materials in organic

Dr. H. Li, Dr. T. Earmme, Dr. S. Subramaniyan, Prof. S. A. Jenekhe
Department of Chemical Engineering and Department of Chemistry
University of Washington
Seattle, WA, 98195-1750, USA
E-mail: jenekhe@u.washington.edu

DOI: 10.1002/aenm.201402041

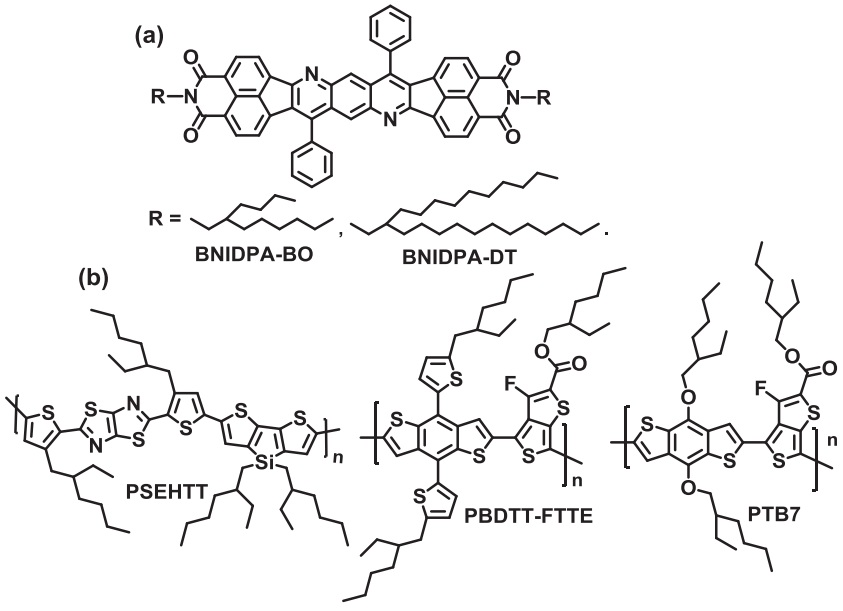

Figure 1. Molecular structures of acceptor molecules BNIDPA-BO and BNIDPA-DT (a) and the donor polymers PSEHTT, PBDTT-FTTE, and PTB7 (b).

light emitting diodes, leading to improved efficiencies and brightness.[49,50] A particularly attractive feature of DPA-containing materials is the relatively facile and scalable synthetic chemistry involving metal catalyst-free Friedlander annulation reaction. However, such prior DPA-containing materials could not be used in BHJ organic solar cells because of their low electron affinities or poor solubility in organic solvents. Herein, we report a novel class of small-molecule nonfullerene acceptors, 2,3,6,7-bis(naphthalene imide)-3,6-diphenyl-*trans*-anthrazolines (BNIDPAs), which gives efficient BHJ solar cells in combination with multiple donor polymers. Two BNIDPA molecules with different alkyl chains, 2-butyloctyl-substituted BNIDPA-BO and 2-decyltetradecyl-substituted BNIDPA-DT (**Figure 1**a), were synthesized to enable the tuning of the solubility, solid-state morphology, and compatability with different donor polymers in BHJ solar cells. The PCE of BHJ solar cells was 3.0% or higher when BNIDPA-BO was paired with each of three common donor polymers, poly[(4,4′-bis(2-ethylhexyl) dithieno[3,2-*b*:2′,3′-*d*]silole)- 2,6-diyl-alt-(2,5-bis(3-(2-ethylhexyl)thiophen-2-yl)thiazolo[5,4-*d*]thiazole)] (PSEHTT),[54,55] poly[4,8-bis(5-(2-ethylhexyl)thiophene-2-yl)benzo[1,2-*b*;4,5-*b*′] dithiophene-2,6-diyl-alt-(4-(2-ethylhexyl)-3-fluorothieno[3,4-*b*] thiophene-)-2-carboxylate-2,6-diyl)] (PBDTT-FTTE),[56–59] or poly[(4,8-bis-(2-ethylhexyloxy)-benzo(1,2-*b*:4,5-*b*′)dithiophene)-2,6-diyl-alt-(4-(2-ethylhexyl)-3-fluorothieno[3,4-*b*]thiophene-)-2-carboxylate-2,6-diyl] (PTB7) (Figure 1b),[60] respectively. In contrast, the efficiencies of the corresponding BNIDPA-DT:donor polymer devices were reduced by a factor of 2, highlighting the critical role of the size of alkyl chains appended to nonfullerene acceptors. We investigated the underlying bulk carrier transport of all six BNIDPA:donor polymer blend systems by the space charge limit current (SCLC) technique and their surface and bulk morphologies by X-ray diffraction (XRD) and atomic force microscopy (AFM) imaging, respectively.

2. Results and Discussion

2.1. Synthesis, Thermal, Optical, and Electrochemical Properties

Scheme 1 shows the synthesis of the BNIDPA molecules. The key monoketone intermediates **2** and **3**, substituted with 2-butyloctyl (BO) and 2-decyltetradecyl (DT), respectively, were synthesized via the oxidation reaction of the corresponding acenaphthene imides.[26] Reaction of monoketones **2** and **3** with 2,5-dibenzoyl-1,4-phenylenediamine (Compound **1**) in toluene using diphenylphosphate (DPP) as the catalyst gave the target BNIDPA-BO or BNIDPA-DT, respectively, in 63%–70% yields. Both BNIDPAs were isolated as bright red solids and their molecular structures were confirmed by ^{1}H and ^{13}C NMR spectra, high resolution mass spectra (HRMS) and elemental analysis. Both BNIDPAs have excellent solubility in organic solvents (chloroform, toluene, chlorobenzene, dichlorobenzene, etc) and are thus suitable for solution-based processing for fabricating devices.

The thermal properties of BNIDPAs were investigated by thermal gravimetric analysis (TGA) and differential scanning calorimetry (DSC). Both BNIDPAs showed good thermal stability with high thermal decomposition temperatures (T_d) at around 460 °C (Figure S3, Supporting Information). DSC scans of BNIDPA-BO in the 30–300 °C range did not show any thermal transitions due to its rigid molecular structure and strong intermolecular interactions (Figure S4, Supporting Information). However, BNIDPA-DT showed a sharp melting transition at 280 °C during the heating scan and a few unresolved crystallization transitions in the 260–210 °C range during the cooling scan (Figure S4, Supporting Information). The observed thermal transitions of BNIDPA-DT originate from its longer and more flexible alkyl chains, which lower the rigidity and intermolecular interactions of the molecules.

Figure 2 presents the UV–vis absorption and photoluminescence (PL) spectra of the BNIDPAs in dilute chloroform solutions and as thin films. As expected from their common π-conjugated framework, BNIDPA-BO and BNIDPA-DT have very similar absorption spectra except that BNIDPA-BO has higher molar extinction coefficient and absorption coefficient.

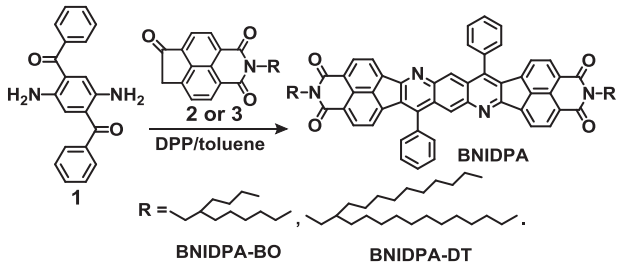

Scheme 1. Synthesis of BNIDPAs via Friedlander annulation reaction.

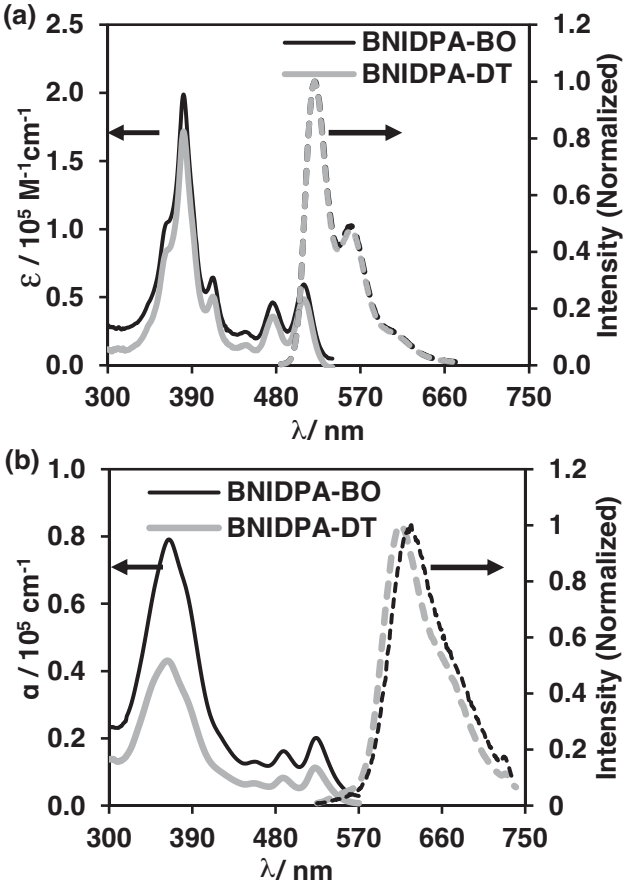

Figure 2. UV–vis absorption [solid lines) and PL [dotted lines) spectra of BNIDPAs in dilute solutions (a) and as thin films (b). Excitation wavelengths were at 380 and 360 nm for PL emission spectra in solution and thin film, respectively.

In dilute solution, the BNIDPA molecules have multiple absorption in the range from 320 to 540 nm with a dominant peak at λ_{max} = 380 nm (ε_{max} = 2.0 × 10^5 cm^{-1} M^{-1} for BNIDPA-BO and 1.6 × 10^5 cm^{-1} M^{-1} for BNIDPA-DT). The thin film absorption bands of BNIDPAs are broader with a λ_{max} = 361 nm, which is 19 nm blue-shifted relative to the solution absorption λ_{max}, suggesting H-aggregation in the solid state. In contrast, the longest wavelength absorption peak appeared at 522 nm in thin films is red-shifted relative to the 0–0 transition peak at 507 nm in dilute solution, which may be due to intermolecular interactions. The optical absorption edge bandgap (E_g^{opt}) of both BNIDPAs as determined from the thin film spectra is 2.22 eV. Both BNIDPAs have identical PL emission spectra with λ_{max} = 538 nm in dilute solution. The thin film PL emission spectra of BNIDPA-BO and BNIDPA-DT have less vibronic structure with a peak at 627 and 615 nm, respectively.

We measured the electronic structure (HOMO/LUMO energy levels) of BNIDPAs by cyclic voltammetry (CV). Both BNIDPAs showed unresolved multiple reduction waves in the range of –1.3–1.6 V versus saturated calomel electrode (SCE), which are due to sequential one-electron reductions of BNIDPA molecules. The LUMO levels of both BNIDPA-BO and BNIDPA-DT were –3.6 eV as determined from the onset reduction potential of the cyclic voltammograms (Figure S5, Supporting Information). This LUMO energy level of the BNIDPA molecules is about 0.7 eV lower lying than that of parent DPA,[50] suggesting that there may be sufficient driving energy for photoinduced electron transfer from many known donor polymers. On the contrary, the LUMO energy of BNIDPA is about 0.3–0.5 eV higher lying than those of PCBMs and thus suggests a potential to achieve higher photovoltages in BNIDPA-based solar cells. Anodic scans up to 1.4 V versus SCE did not show any oxidation events, suggesting that the HOMO energy levels of BNIDPA should be below –6.0 eV. The HOMO energy level directly determined by CV is thus expected to be deeper than that –5.8 eV determined from the LUMO energy level and E_g^{opt} (2.22 eV).

2.2. Theoretical Calculations

The geometry optimization was carried on the model molecule BNIDPA-M2 with two appended methyl groups to simplify the calculations using density functional theory (DFT) at the B3LYP/6–31G(d) level. As expected, the ladder-type core of 2,3,6,7-bis(naphthalene imide)-*trans*-anthrazoline (BNIA) is perfectly planar with a long π-conjugated framework of ≈2.0 nm (**Figure 3**). The two phenyl groups attached at the bay positions are strongly twisted with interplanar angles of over 70° between phenyl and the BNIA core (Figure 3 and Table S1, Supporting Information). The frontier orbital energy levels BNIDPA-M2 and the low lying excited states of the corresponding mono-anion were also calculated at the same B3LYP/6–31G(d) level and are shown in **Figure 4**. BNIDPA has three quasi-degenerate LUMOs at –2.64 to –3.05 eV range (Figure 4a), whereas its anion has two low energy excited states (Figure 4b). The presence of multiple electron accepting states in BNIDPA-M2, similar to $PC_{60}BM$, is expected to benefit efficient charge separation in BHJ OPVs.[61]

2.3. BHJ Polymer Solar Cells

The HOMO/LUMO energy levels of the donor polymers (PSEHTT, PBDTT-FTTE, and PTB7) selected to evaluate the photovoltaic properties of the new acceptor materials are shown in **Figure 5**a in comparison to those of the BNIDPAs. BHJ solar cells with the structure of ITO/zinc oxide (ZnO)/BNIDPA:donor polymer/molybdenum oxide (MoO_3)/Ag (Figure 5b) were fabricated and evaluated. The current density (*J*)–voltage (*V*) characteristics were measured under AM 1.5G solar illumination at 1 sun (100 mW cm^{-2}) in ambient air. The optimal performance of BNIDPA-BO:PSEHTT blend devices was achieved at 4:1 (wt/wt) with a PCE of 3.02%, short-circuit current density (J_{sc}) of 6.64 mA cm^{-2}, open-circuit voltage (V_{oc}) of 0.94 V, fill factor (FF) of 0.48 (Figure 5c, **Table 1**). BNIDPA-BO:PBDTTT-FTTE (3:1 wt/wt) devices gave the highest PCE of 3.00% with J_{sc} of 9.02 mA cm^{-2}, V_{oc} of 0.96 V, and FF of 35% (Figure 5e and Table 1). The optimal BNIDPA-BO:PTB7 devices were also at 3:1 (wt/wt), giving 3.08% PCE with J_{sc} of 8.13 mA cm^{-2}, V_{oc} of 0.98 V and FF of 39% (Figure 5g and Table 1). We note that BNIDPA-BO:PBDTT-FTTE, BNIDPA-BO:PTB7, and

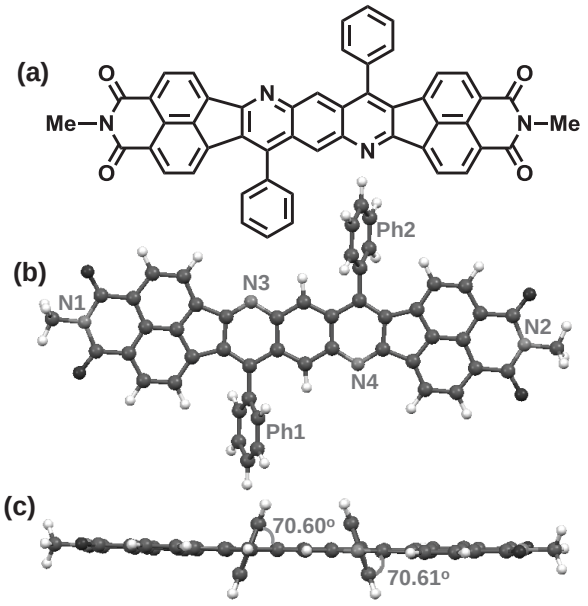

Figure 3. Molecular structure of methyl substituted BNIDPA-M2 (2-DT or 2-BO were replaced by methyl to simplify the calculation) (a). Top (b) and side view (c) of optimized BNIDPA-M2 using DFT calculations at the B3LYP/6–31G(d) level.

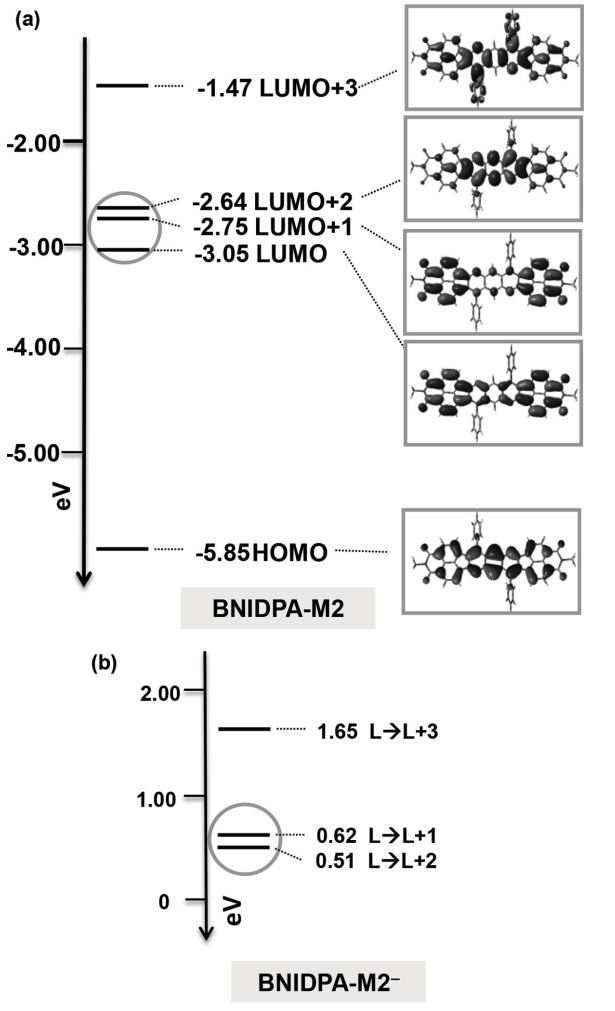

Figure 4. Calculated quasi degenerate LUMO energy levels and the corresponding orbital surface of the optimized BNIDPA-M2 (a) and low lying excited states of BNIDPA-M2 monoanion (b) using DFT calculations (B3LYP/6–31G]d).

BNIDPA-BO:PSEHTT devices all showed high open-circuit voltages of close to 1.0 V, which are 0.2–0.3 V higher than the corresponding $PC_{60}BM$ and $PC_{70}BM$ devices with the same donor polymers[54,55,60] and are rarely achieved in ubiquitous NDI/PDI devices; [15–24,31,33,39–41,43,46,47] the high V_{oc}s are largely due to the relatively high lying LUMO of BNIDPA-BO compared with the PCBMs or NDI/PDI derivative small molecules or polymers. We also highlight the fact that all BHJ solar cells pairing the new electron acceptor BNIDPA-BO with three different donor polymers (PSEHTT, PBDTT-FTTE, and PTB7, respectively) have PCEs of 3.0%–3.1%.

Although a prior report has demonstrated the use of a nonfullerene acceptor to realize BHJ solar cells with four different donor polymers, the PCEs achieved were less than 1.5%.[23] Another prior report has also used a nonfullerene acceptor to make BHJ devices with one donor polymer and a donor small molecule, achieving PCEs of 2.6% and 3.1%, respectively.[33] The present efficiency (≥3.0%) of BNIDPA-BO BHJ solar cells with multiple donor polymers are without precedence and thus they help to advance toward the realization of universally applicable electron-acceptor materials for efficient nonfullerene solar cells.[23]

The external quantum efficiency (EQE) spectra corresponding to the optimal BNIDPA-BO BHJ devices are also shown in Figure 5. The EQE spectrum of BNIDPA-BO:PSEHTT covers the 300–700 nm range with comparable 42%–46% peak values in the 300–450 nm and the 450–700 nm regions that correspond to the overlaid absorption spectra of the donor material BNIDPA-BO and the donor polymer PSEHTT (Figure 5d). The J_{sc} calculated from the EQE spectrum is 6.41 mA cm^{-2}, which is within 3% of the direct J–V measurement. The EQE spectra of BNIDPA-BO:PBDTT-FTTE (Figure 5f) and BNIDPA-BO:PTB7 (Figure 5h) extended to longer wavelength of ≈780 and ≈750 nm, respectively, which are consistent with the low-energy optical absorption spectra of these donor polymers (Figure S10, Supporting Information). The EQE spectrum of BNIDPA-BO:PBDTT-FTTE devices has peaks of 45% in the 480–520 nm region and 44% in the 600–740 nm region, while that of BNIDPA-BO:PTB7 devices has lower peaks of 44% in the 480–520 nm region and 38% in the 600–720 nm region. The current densities calculated from the EQE spectra are 8.83 mA cm^{-2} for BNIDPA-BO:PBDTT-FTTE and 7.73 mA cm^{-2} for BNIDPA-BO:PTB7, which are in good agreement with those from direct J–V measurements.

The photovoltaic properties of BNIDPA-DT paired with different donor polymers, PSEHTT, PBDTT-FTTE, and PTB7, were similarly evaluated. The measured J–V curves and EQE spectra are also shown in Figure 5. The solar cell parameters, J_{sc}, V_{oc}, FF, and PCE, are summarized in Table 1. Compared with BNIDPA-BO devices, the optimal BNIDPA-DT:PSEHTT, BNIDPA-DT:PBDTT-FTTE, and BNIDPA-DT:PTB7 blend devices have comparable V_{oc} (0.94–0.95 V) and

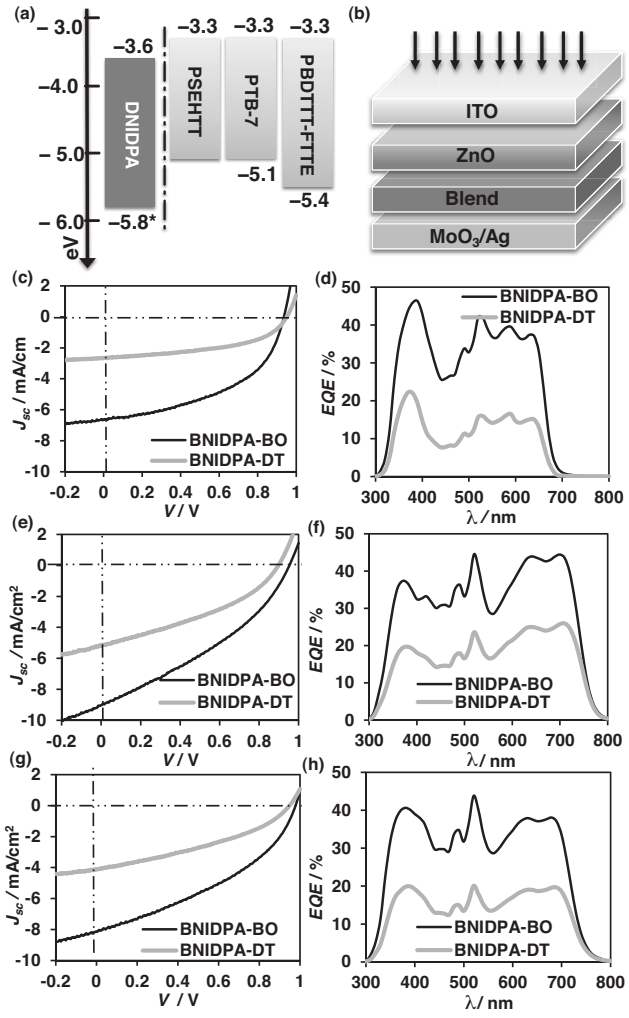

Figure 5. The frontier molecular orbital energy levels of BNIDPAs in comparison to that of PSEHTT, PBDTT-FTTE, and PTB7 [*The HOMO energy level of BNIDPA is calculated from LUMO and E_g, and it is deeper than –6.0 eV from cyclic voltammetry) (a), schematic of inverted cell (b), *J*–*V* curves (c,e,g) and EQE spectra (d,f,h) of inverted solar cells based on the BNIDPA-BO:PSEHTT [4:1 wt/wt) (c,d), BNIDPA-DT:PBDTT-FTTE (3:1 wt/wt) (e,f) and BNIDPA-BO:PTB7 (3:1 wt/wt) (g,h) blends.

FF (36%–50%), but significantly lower short-circuit currents (2.67–5.20 mA cm^{-2}), leading to significantly lower PCEs of 1.26%–1.71% (Table 1). The EQE of BNIDPA-DT:PSEHTT, BNIDPA-DT:PBDTT-FTTE, and BNIDPA-DT:PTB7 devices are significantly lower than those of the corresponding BNIDPA-BO devices (Figure 5). The observed low photocurrents in BNIDPA-DT devices arise from a number of factors due to the large alkyl chains, including: (i) the smaller absorption coefficient and thus poorer light harvesting efficiency (Figure 2b); (ii) inefficient intermolecular electronic coupling and thus lower electron mobility; and (iii) possibly also blend morphology since BNIDPA-BO more readily crystalizes than BNIDPA-DT as will be discussed in the next section. The observed significantly better photovoltaic properties of BNIDPA-BO solar cells compared with those composed of the BNIDPA-DT acceptor highlight the important role of alkyl chains appended to nonfullerene acceptors. Although side chains have been widely recognized as important variables in tuning and optimizing the photovoltaic properties of donor or acceptor polymers,[39–41,43,54] we are not aware of any prior report of such a large effect of alkyl chains on the photovoltaic properties of small-molecule nonfullerene acceptors. We suggest that optimal choice of side chains appended onto nonfullerene acceptors has the potential to significantly improve the performance of current nonfullerene BHJ solar cells.

Finally, we note that the FFs of all the present nonfullerene BHJ solar cells (FF = 35%–48% for BNIDPA-BO and FF = 36%–50% for BNIDPA-DT) are relatively low compared with the corresponding PCBM devices based on the same donor polymers (FF = 69%–74%).[61,62,67] Low FF values in BHJ polymer solar cells are generally due to high geminate and bimolecular recombination rates, which could be significantly reduced by improving the bulk nanoscale morphology through processing (e.g., by using processing additives),[15,18,62–64] control of blend phase segregation,[18,40,62–65] and interface engineering with additional electron/hole transport layers.[31,39,40,65,66]

2.4. Bulk Charge Transport and Solid State Morphology of Active BHJ Layer

We used SCLC measurements to investigate the bulk charge transport in the BNIDPA blend devices toward a better understanding of the photovoltaic properties. Hole-only devices with the structure of ITO/PEDOT:PSS/blend/Au and electron-only devices with the structure of ITO/ZnO/blend/LiF/Al were fabricated and characterized (Figure S6, Supporting Information). The resulting hole and electron mobilities of the six blend systems consisting of two acceptor materials (BNIDPA-BO and BNIDPA-DT) and three donor polymers (PSEHTT, PBDTT-FTTE, and PTB7) are summarized in Table 1. The observed hole mobility of the blends is largely independent of the acceptor component: 2.5×10^{-4}–3.4×10^{-4} cm^2 V^{-1} s^{-1} for PSEHTT blends; 5.8×10^{-4}–6.8×10^{-4} cm^2 V^{-1} s^{-1} for PBDTT-FTTE blends; and 2.2×10^{-4}–2.4×10^{-4} cm^2 V^{-1} s^{-1} for PTB7 blends. It is interesting that hole mobilities observed here for PSEHTT, PBDTT-FTTE, and PTB7, respectively, are quite comparable to values reported for other acceptor:polymer solar cells. For example, an SCLC hole mobility of 5.8×10^{-4} cm^2 V^{-1} s^{-1} was observed in $PC_{70}BM$:PTB7 blends,[67] and 2.6×10^{-4}–5.4×10^{-4} cm^2 V^{-1} s^{-1} in all-polymer blends containing PSEHTT.[40] In contrast, the electron mobility of BNIDPA-BO blends varies significantly from 5.4×10^{-6} cm^2 V^{-1} s^{-1} in PSEHTT blends to 6.0×10^{-5} cm^2 V^{-1} s^{-1} in PBDTT-FTTE blends. The bulk electron mobility in these BNIDPA-BO binary blends with the three donor polymers are factors of 5–63 smaller than the corresponding hole mobility (Table 1), clearly demonstrates substantial imbalance in carrier transport in the BHJ solar cells, which can largely explain the low FFs.[64,65] The observed bulk electron mobilities in all the BNIDPA-BO:polymer blends are also substantially lower than those observed in the corresponding $PC_{60}BM$:polymer blends, which can also explain the lower performance of the BNIDPA-BO devices compared with the $PC_{70}BM$ devices.[54–60]

Table 1. Photovoltaic properties of BNIDPA:donor BHJ solar cells and SCLC carrier mobilities of the BNIDPA:donor polymer blend active layers.

Acceptor	Donor	J_{sc} [mA cm^{-2}]	V_{oc} [V]	FF [%]	PCE_{max} [%]	PCE_{ave}[d)] [%]	μ_h [cm^2 V^{-1} s^{-1}]	μ_e [cm^2 V^{-1} s^{-1}]
BNIDPA-BO	PSEHTT[a)]	6.64	0.94	48	3.02	2.87 ± 0.13	3.4×10^{-4}	5.4×10^{-6}
	PBDTT-FTTE[b)]	9.02	0.96	35	3.00	2.91 ± 0.08	6.8×10^{-4}	6.0×10^{-5}
	PTB7[c)]	8.13	0.98	39	3.08	2.90 ± 0.15	2.4×10^{-4}	5.2×10^{-5}
BNIDPA-DT	PSEHTT[a)]	2.67	0.95	50	1.26	1.16 ± 0.08	2.5×10^{-4}	4.5×10^{-8}
	PBDTT-FTTE[b)]	5.20	0.90	36	1.71	1.60 ± 0.09	5.8×10^{-4}	2.7×10^{-6}
	PTB7[c)]	4.12	0.95	36	1.42	1.32 ± 0.09	2.2×10^{-4}	2.5×10^{-6}

[a)]The active layer was deposited from BNIDPA:PSEHTT (4:1 wt/wt) solution in chloroform followed by thermal annealing at 175 °C for 10 min; [b)]The active layer was deposited from BNIDPA:PBDTT-FTTE (3:1 wt/wt) solution in chlorobenzene and dichlorobenzene (9:1 *v/v*); [c)]The active layer was deposited from BNIDPA:PTB7 (3:1 wt/wt) solution in chlorobenzene and dichlorobenzene (9:1 *v/v*); [d)]from five devices.

The observed bulk electron mobilities of BNIDPA-DT:polymer blends are about 1–2 orders of magnitude lower than those of the corresponding BNIDPA-BO blends. This observation largely accounts for the poorer photocurrent and efficiency of BNIDPA-DT BHJ solar cells compared with those of BNIDPA-BO devices. The much lower electron mobility in BNIDPA-DT blends arises from poorer intermolecular electronic coupling because of the longer alkyl chains. These results demonstrate the critical role of the size of alkyl chains appended onto nonfullerene acceptors on the bulk charge transport and photovoltaic properties of BHJ solar cells using them.

The surface morphology of the actual BHJ devices based on six BNIDPA-BO:polymer and BNIDPA-DT:polymer blend systems was investigated by AFM imaging. The height and phase images (5 μm × 5 μm) of BNIDPA-BO blends are shown in **Figure 6**. The BNIDPA-BO:PSEHTT blend has a smooth surface with a small roughness (R_g) of 0.41 nm (Figure 6a) and small phase-separated domains (20–50 nm) (Figures 6b and S6, Supporting Information). In comparison, the BNIDPA-BO:PBDTT-FTTE blend has a slightly more rough surface (R_g = 1.2 nm) (Figure 6c) with larger phase-separated domains (Figure 6d). The surface morphology of BNIDPA-BO:PTB7 blend seen in both height and phase images (Figure 6e,f) reveals a fabric-like pattern, with a R_g of 0.51 nm, which is different from the other BNIDPA-BO:polymer blends. The AFM height and phase images of BNIDPA-DT:polymer blend devices are shown in Figure S9 (Supporting Information). The surface morphologies revealed in these AFM images of BNIDPA-DT:polymer blend devices are very similar to their corresponding BNIDPA-BO:polymer blends. We conclude that the surface morphologies revealed by AFM imaging do not provide explanation for the far superior photovoltaic properties of BNIDPA-BO:polymer devices compared with the corresponding BNIDPA-DT devices.

We investigated the solid-state morphologies of the BNIDPA-BO:polymer and BNIDPA-DT:polymer blend systems by XRD and the diffraction patterns are shown in **Figures 7** and S5 (Supporting Information). A lamellar crystalline (100) reflection peak at 5.0° (d = 17.7 Å) was observed in neat films of PSEHTT, whereas no diffraction peaks were seen in neat films of either PBDTT-FTTE or PTB7, indicating that these later polymers form amorphous films (Figure S7, Supporting Information). A neat film of BNIDPA-BO has two major diffraction peaks at 4.38° (d = 20.2 Å) and 7.56° (d = 11.7 Å) (Figure S7, Supporting Information), which are assigned to diffractions along the long and short molecular axes of BNIDPA-BO, respectively, by comparing to the calculated dimensions (Table S1, Supporting Information). These two diffraction peaks were also observed in the BNIDPA-BO:polymer blend films, appearing at 4.38°–4.60° (d = 20.2 Å–19.2 Å) and 7.56° (d = 11.2 Å) (Figure 7). This is an indication that BNIDPA-BO:polymer blends are phase-separated

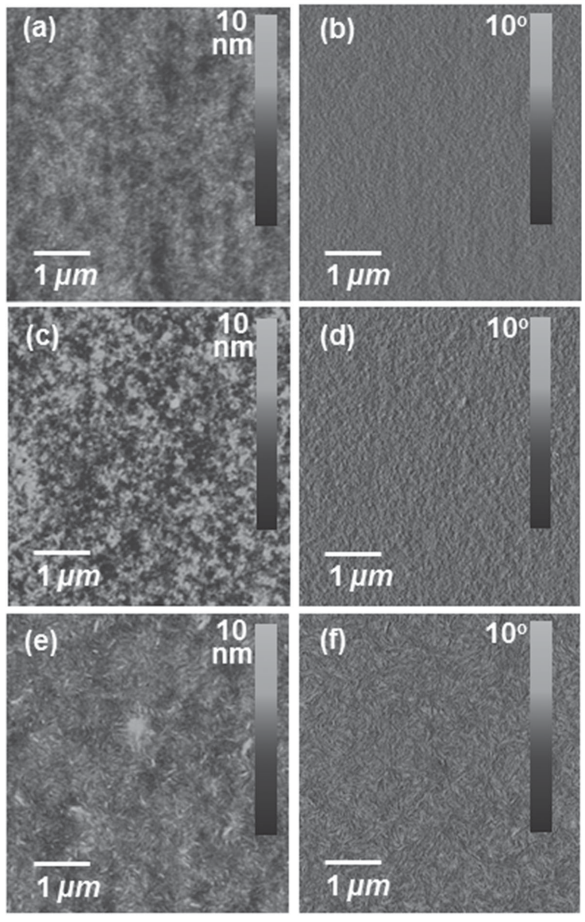

Figure 6. AFM height (a,c,e) and phase (b,d,f) images of the actual devices based on BNIDPA-BO:PSEHTT (a,b), BNIDPA-BO:PBDTT-FTTE (c,d) and BNIDPA-BO:PTB7 (e,f).

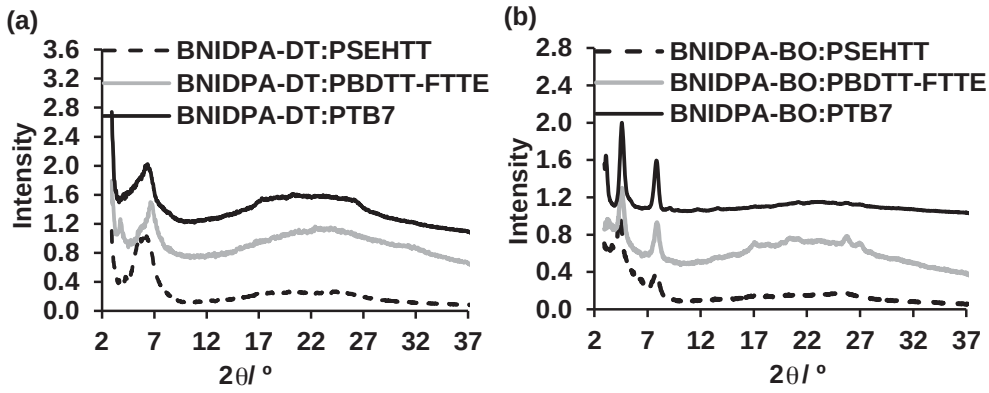

Figure 7. XRD patterns of drop-casted BNIDPA-BO:donor polymer (a) and BNIDPA-DT:donor polymer (b) blend films BNIDPA:PSEHTT (4:1 wt/wt), BNIDPA:PBDTT-FTTE (3:1 wt/wt) and BNIDPA:PTB7 (3:1 wt/wt).

with largely pure BNIDPA-BO acceptor domains since the diffraction signals of BNIDPA-BO in both neat and blend films are intense and relatively sharp. The (100) lamellar diffraction peak seen in neat PSEHTT films was not observed in the BNIDPA-BO:PSEHTT blends due to the lower weight ratio and relatively poorer crystallinity of the donor component.

BNIDPA-DT neat films have two XRD peaks at 3.50° and 7.02°, corresponding to the 1st and 2nd order diffractions (d = 25.2 Å) along the long molecular axis of the BNIDPA-DT, respectively, whereas the diffraction along the short molecular axis was not observed. The two diffractions observed in the BNIDPA-DT neat films were also seen in the corresponding BNIDPA-DT:polymer blend films appearing at 6.3°–6.7° (d = 28.0–26.4 Å). The shift (about 3–1 Å) of the diffraction peaks observed in BNIDPA-DT blend relative to the BNIDPA-DT neat film suggests that the acceptor domains in the blend films may contain some donor components. For BNIDPA-DT:PSEHTT blend, the diffraction signal in 5°–7° may also contain the (100) diffraction of PSEHTT (Figure S7, Supporting Information). The observed diffraction peaks in BNIDPA-DT:polymer blends are weaker, broader, and correspond to larger d-spacings, in comparison to those of BNIDPA-BO:polymer blends. These data indicate that BNIDPA-DT is less crystalline, and thus explain the lower bulk electron mobilities and photocurrents in BNIDPA-DT:polymer blends. The fact that some crystalline BNIDPA-DT-rich domains may also contain donor polymer molecules also suggests increased charge recombination, which further accounts for the observed low-efficiencies (<2%) of BNIDPA-DT BHJ solar cells.

3. Conclusions

A new class of nonfullerene acceptors, 2,3,6,7-BNIDPAs, suitable for use with multiple donor polymers in BHJ organic solar cells has been developed and presented. Two BNIDPA molecules, 2-butyloctyl-substituted BNIDPA-BO and 2-decyltetrdecyl-substituted BNIDPA-DT, were synthesized and used to investigate the effects of the size of alkyl chains on the solid-state morphology, bulk charge transport, and photovoltaic properties of BNIDPA:polymer BHJ solar cells. Inverted BHJ devices composed of binary blends of BNIDPA-BO acceptor with donor polymer PSEHTT, PBDTT-FTTE, and PTB7, respectively were found to have 3.0%–3.1% PCE and high open-circuit voltages (≈1 V). Similar BHJ devices replacing BNIDPA-BO with BNIDPA-DT acceptor had about twofold reduction in photovoltaic efficiency and up to two orders of magnitude reduction in bulk electron mobility, demonstrating the critical role of the size of alkyl chains appended onto nonfullerene acceptors. EQE spectra of the BHJ polymer solar cells show that BNIDPA acceptors significantly contributed to light harvesting and photocurrent generation. These results demonstrate that unlike most current nonfullerene electron acceptors, BNIDPA-BO exemplifies those applicable to multiple donor polymers for the development of efficient nonfullerene OPV.

4. Experimental Section

Materials: Diphenylphosphate (DPP) was purchased from Aldrich and used as received. 2,5-Dibenzoyl-1,4-phenylenediamine,[56] *N*-2-BO-1,8-dihydroacenaphthalene-4,5-dicarboxylic acid imide,[26] and *N*-2-decyltetradecyl-1,8-dihydroacenaphthalene-4,5-dicarboxylic acid imide[26] were synthesized by following the reported procedures.

Synthesis of BNIDPA-BO: Under argon, monoketone **2** (250 mg, ≈50%), (2,5-diamino-1,4-phenylene)bis(phenylmethanone) (39 mg, 0.12 mmol) and diphenyl phosphate (800 mg) and toluene (5 mL) were transferred into a Schlenk reaction tube. The tube was closed; the mixture was slowly warmed up to 110 °C and kept stirring overnight. After cooling back to room temperature, the dark red solution was precipitated into methanol (80 mL) and triethylamine mixture (2:1, *v*/*v*). A red solid formed, was collected and washed with methanol (3 × 20 mL). The solid was further purified by column chromatography with $CHCl_3$ as the eluent solvent. Yield: 91 mg. ^{1}H NMR ($CDCl_3$, 500 MHz, δ): 8.27 (d, 2H, ^3J = 7.5 Hz, Np), 8.23 (s, 2H, An), 7.91 (t, 4H, ^3J = 7.5 Hz, Ph), 7.83 (t, 6H, ^3J = 7.5 Hz, Ph), 7.73 (d, 2H, ^3J = 6.5 Hz, Np), 7.45 (d, 2H, ^3J = 8.0 Hz, Np), 6.97 (d, 2H, ^3J = 7.5, Np), 4.10 (d, 4H, ^3J = 7.0 Hz, CH_2), 1.90 (m, 2H, CH), 1.4–1.2 (m, 32H, CH_2), 1.0–0.8 (m, 12H, CH_3). ^{13}C NMR ($CDCl_3$, 125.7 MHz, δ): 163.5, 163.3, 159.9, 144.1, 144.0, 138.4, 138.3, 134.8, 134.3, 132.4, 130.9, 130.0, 129.8, 129.4, 129.2, 128.6, 127.8, 124.7, 123.2, 122.9, 122.2, 120.9, 44.7, 36.9, 32.1, 32.0, 31.6, 30.0, 29.0, 26.8, 23.3, 22.9, 14.3; HRMS (m/z): $[M]^+$ calcd. for $C_{72}H_{70}N_4O_4$, 1054.54; found, 1055.50. Elemental analysis calcd for $C_{80}H_{86}N_4O_4$: C 81.94%, H 6.69%, and N 5.31%; found C 81.38%, H 6.71%, and N 5.10%.

Synthesis of BNIDPA-DT: Under argon, monoketone **3** (300 mg, ≈50%), (2,5-diamino-1,4-phenylene)bis(phenylmethanone) (27.5 mg, 0.087 mmol), diphenyl phosphate (800 mg), and toluene (5 mL) were transferred into a Schlenk reaction tube. The tube was closed; the

mixture was slowly warmed up to 110 °C and kept stirring overnight. After cooling back to room temperature, the dark red solution was precipitated into methanol (80 mL) and triethylamine mixture (2:1, *v*/*v*). A red solid formed, was collected and washed with methanol (3 × 20 mL). The solid was further purified by column chromatography with $CHCl_3$ as the eluent solvent. Yield: 76 mg. ^{1}H NMR ($CDCl_3$, 500 MHz, δ): 8.26 (d, 2H, ^3J = 7.5 Hz, Np), 8.22 (s, 2H, An), 7.91 (t, 4H, ^3J = 7.5 Hz, Ph), 7.82 (t, 6H, ^3J = 7.5 Hz, Ph), 7.71 (d, 2H, ^3J = 6.5 Hz, Np), 7.43 (d, 2H, ^3J = 7.0 Hz, Np), 6.97 (d, 2H, ^3J = 7.5, Np), 4.09 (d, 4H, ^3J = 7.0 Hz, CH_2), 1.90 (m, 2H, CH), 1.4–1.2 (m, 80H, CH_2), 1.0–0.8 (m, 12H, CH_3). ^{13}C NMR ($CDCl_3$, 125.7 MHz, δ): 163.5, 163.2, 159.8, 144.1, 143.9, 138.4, 138.2, 134.7, 134.3, 132.4, 130.9, 129.9, 129.8, 129.4, 129.2, 128.6, 127.7, 124.6, 123.2, 122.9, 122.2, 120.9, 44.8, 36.9, 32.1, 32.0, 30.3, 29.9 (2), 29.6, 26.8, 22.9, 14.3; HRMS (m/z): $[M]^+$ calcd. for $C_{96}H_{118}N_4O_4$, 1391.92; found, 1392.66. Elemental analysis calcd for $C_{96}H_{118}N_4O_4$: C 82.83%, H 8.54%, and N 4.02%; found C 82.83%, H 8.48%, and N 4.10%.

Fabrication of BHJ Solar Cells: ZnO precursor solution was prepared by dissolving zinc acetate dihydrate (1 g, 99.999% trace metals basis, Aldrich) in 2-methoxyethanol (10 mL, 99.8%, anhydrous, Aldrich) followed by adding ethanolamine (0.28 g, ≥99.5%, Aldrich) under stirring for overnight in ambient conditions. Ethanolamine, 2-methoxylethanol and chloroform (Sigma-Aldrich) were used as received. ITO glass substrate was cleaned sequentially in ultrasonic baths of acetone and isopropanol and then dried at 60 °C in a vacuum oven overnight. The substrate was O_2 plasma treated right before use. The ZnO precursor solution was spin-coated onto the ITO glass at 5000 rpm for 60 s and annealed at 250 °C for 1 h to make ≈30-nm thick ZnO layer. A solution of 1 vol% ethanolamine in 2-methoxyethanol was spin-coated onto the ZnO layer and dried at 110 °C for 10 min. The BNIDPA:PSEHTT active layer was spin-coated from the BNIDPA:PSEHTT blend (4:1, wt/wt) solution in $CHCl_3$. After spin-coating, the film was annealed at 175 °C for 10 min inside a glovebox. The BNIDPA:PBDTT-FTTE and BNIDPA:PTB7 active layers were spin-coated from the BNIDPA:PBDTT-FTTE (3:1, wt/wt) and BNIDPA:PTB7 (3:1, wt/wt) blend solutions in chlorobenzene and dichlorobenzene mixture (9:1, *v*/*v*), respectively. The substrates were then loaded in a thermal evaporator (BOC Edwards, 306) to deposit a cathode composed MoO_3 (5.0 nm) and Ag (100 nm) under high vacuum (8×10^{-7} Torr). Five solar cells, each with an active area of 4 mm^2, were fabricated per ITO substrate. The current density–voltage (*J*–*V*) curves of solar cells were measured using a HP4155A semiconductor parameter analyzer under laboratory ambient air conditions. An AM 1.5G illumination at 100 mW cm^{-2} was provided by a filtered Xe lamp and calibrated by using an NREL-calibrated Si photodiode. The external quantum efficiency (EQE) was measured by using a QEX10 solar cell quantum efficiency measurement system (PV Measurements, Inc.) and was calibrated with a NREL-certified Si photodiode before measurement.

Space-Charge-Limited Current (SCLC) Measurement: The current density–voltage (*J*–*V*) characteristics of the SCLC devices were measured by using a HP4155A semiconductor parameter analyzer (Yokogawa Hewlett-Packard, Tokyo). Hole-only devices with the structure of ITO/PEDOT:PSS/blend/Au and electron-only devices with the structure of ITO/ZnO/blend/MoO_3/Ag were fabricated and characterized. The carrier mobility was extracted by fitting the *J*–*V* curves in the near quadratic region according to the modified Mott–Gurney equation[67]

$$J = \frac{9}{8}\varepsilon\varepsilon_0\,\mu\frac{V^2}{L^3}\exp\left(0.89\beta\frac{\sqrt{V}}{\sqrt{L}}\right) \quad (1)$$

where J is the current density, ε_0 is the permittivity of free space, ε is the relative permittivity, μ is the zero-field mobility, V is the applied voltage, L is the thickness of active layer, and β is the field-activation factor.

Supporting Information

Supporting Information is available from the Wiley Online Library or from the author.

Acknowledgements

The authors thank Matthew J. Crane for discussion and Mingqian Zhang and Minako Goh for help with the synthesis of monoketones. This work was supported by the NSF (Grant No. CBET-1435912) and in part by the Office of Naval Research (ONR) (Grant No. N00014–11–1–0317).

Received: November 14, 2014
Revised: December 11, 2014
Published online: January 8, 2015

[1] A. Facchetti, *Mater. Today* **2013**, *16*, 123.
[2] C. R. McNeill, *Energy Environ. Sci.* **2012**, *5*, 5653.
[3] Y. Lin, X. Zhan, *Mater. Horizons* **2014**, *1*, 470.
[4] A. a. F. Eftaiha, J.-P. Sun, I. G. Hill, G. C. Welch, *J. Mater. Chem. A* **2014**, *2*, 1201.
[5] P. Sonar, J. P. Fong Lim, K. L. Chan, *Energy Environ. Sci.* **2011**, *4*, 1558.
[6] J. E. Anthony, *Chem. Mater.* **2011**, *23*, 583.
[7] M. M. Alam, S. A. Jenekhe, *Chem. Mater.* **2004**, *16*, 4647.
[8] P. E. Schwenn, K. Gui, A. M. Nardes, K. B. Krueger, K. H. Lee, K. Mutkins, H. Rubinstein-Dunlop, P. E. Shaw, N. Kopidakis, P. L. Burn, P. Meredith, *Adv. Energy Mater.* **2011**, *1*, 73.
[9] F. G. Brunetti, X. Gong, M. Tong, A. J. Heeger, F. Wudl, *Angew. Chem Int. Ed.* **2010**, *49*, 532.
[10] C. H. Woo, T. W. Holcombe, D. A. Unruh, A. Sellinger, J. M. J. Fréchet, *Chem. Mater.* **2010**, *22*, 1673.
[11] T. Zhou, T. Jia, B. Kang, F. Li, M. Fahlman, Y. Wang, *Adv. Energy Mater.* **2011**, *1*, 431.
[12] Y. Zhou, L. Ding, K. Shi, Y.-Z. Dai, N. Ai, J. Wang, J. Pei, *Adv. Mater.* **2012**, *24*, 957.
[13] Y. Zhou, Y.-Z. Dai, Y.-Q. Zheng, X.-Y. Wang, J.-Y. Wang, J. Pei, *Chem. Commun.* **2013**, *49*, 5802.
[14] Y.-Q. Zheng, Y.-Z. Dai, Y. Zhou, J.-Y. Wang, J. Pei, *Chem. Commun.* **2014**, *50*, 1591.
[15] A. Sharenko, D. Gehrig, F. Laquai, T.-Q. Nguyen, *Chem. Mater.* **2014**, *26*, 4109.
[16] X. Zhang, Z. Lu, L. Ye, C. Zhan, J. Hou, S. Zhang, B. Jiang, Y. Zhao, J. Huang, S. Zhang, Y. Liu, Q. Shi, Y. Liu, J. Yao, *Adv. Mater.* **2013**, *25*, 5791.
[17] Y. Lin, P. Cheng, Y. Li, X. Zhan, *Chem. Commun.* **2012**, *48*, 4773.
[18] G. Ren, E. Ahmed, S. A. Jenekhe, *Adv. Energy Mater.* **2011**, *1*, 946.
[19] E. Ahmed, G. Ren, F. S. Kim, E. C. Hollenbeck, S. A. Jenekhe, *Chem. Mater.* **2011**, *23*, 4563.
[20] R. Shivanna, S. Shoaee, S. Dimitrov, S. K. Kandappa, S. Rajaram, J. R. Durrant, K. S. Narayan, *Energy Environ. Sci.* **2014**, *7*, 435.
[21] W. Jiang, L. Ye, X. Li, C. Xiao, F. Tan, W. Zhao, J. Hou, Z. Wang, *Chem. Commun.* **2014**, *50*, 1024.
[22] Y. Lin, Y. Wang, J. Wang, J. Hou, Y. Li, D. Zhu, X. Zhan, *Adv. Mater.* **2014**, *26*, 5137.
[23] T. V. Pho, F. M. Toma, B. J. Tremolet de Villers, S. Wang, N. D. Treat, N. D. Eisenmenger, G. M. Su, R. C. Coffin, J. D. Douglas, J. M. J. Fréchet, G. C. Bazan, F. Wudl, M. L. Chabinyc, *Adv. Energy Mater.* **2014**, *4*, 1301007.
[24] A. Sharenko, C. M. Proctor, T. S. van der Poll, Z. B. Henson, T.-Q. Nguyen, G. C. Bazan, *Adv. Mater.* **2013**, *25*, 4403.
[25] J. T. Bloking, X. Han, A. T. Higgs, J. P. Kastrop, L. Pandey, J. E. Norton, C. Risko, C. E. Chen, J.-L. Brédas, M. D. McGehee, A. Sellinger, *Chem. Mater.* **2011**, *23*, 5484.
[26] H. Li, F. S. Kim, G. Ren, E. C. Hollenbeck, S. Subramaniyan, S. A. Jenekhe, *Angew. Chem Int. Ed.* **2013**, *52*, 5513.
[27] J. T. Bloking, T. Giovenzana, A. T. Higgs, A. J. Ponec, E. T. Hoke, K. Vandewal, S. Ko, Z. Bao, A. Sellinger, M. D. McGehee, *Adv. Energy Mater.* **2014**, 1301426.

[28] K. N. Winzenberg, P. Kemppinen, F. H. Scholes, G. E. Collis, Y. Shu, T. Birendra Singh, A. Bilic, C. M. Forsyth, S. E. Watkins, *Chem. Commun.* **2013**, *49*, 6307.
[29] Z. Mao, W. Senevirathna, J.-Y. Liao, J. Gu, S. V. Kesava, C. Guo, E. D. Gomez, G. Sauvé, *Adv. Mater.* **2014**, *26*, 6290.
[30] O. K. Kwon, J.-H. Park, S. K. Park, S. Y. Park, *Adv. Energy Mater.* **2014**, *4*, 1400929.
[31] Y. Zang, C.-Z. Li, C.-C. Chueh, S. T. Williams, W. Jiang, Z.-H. Wang, J.-S. Yu, A. K. Y. Jen, *Adv. Mater.* **2014**, *26*, 5708.
[32] H. Li, T. Earmme, G. Ren, A. Saeki, S. Yoshikawa, N. M. Murari, S. Subramaniyan, M. J. Crane, S. Seki, S. A. Jenekhe, *J. Am. Chem. Soc.* **2014**, *136*, 14589.
[33] Y. Lin, J. Wang, S. Dai, Y. Li, D. Zhu, X. Zhan, *Adv. Energy Mater.* **2014**, *4*, 1400420.
[34] P. E. Hartnett, A. Timalsina, H. S. S. R. Matte, N. Zhou, X. Guo, W. Zhao, A. Facchetti, R. P. H. Chang, M. C. Hersam, M. R. Wasielewski, T. J. Marks, *J. Am. Chem. Soc.* **2014**, *136*, 16345.
[35] Y. Zhong, M. T. Trinh, R. Chen, W. Wang, P. P. Khlyabich, B. Kumar, Q. Xu, C.-Y. Nam, M. Y. Sfeir, C. Black, M. L. Steigerwald, Y.-L. Loo, S. Xiao, F. Ng, X. Y. Zhu, C. Nuckolls, *J. Am. Chem. Soc.* **2014**, *136*, 15215.
[36] L. Ye, W. Jiang, W. Zhao, S. Zhang, D. Qian, Z. Wang, J. Hou, *Small* **2014**, *10*, 4658.
[37] X. Zhang, Z. Lu, L. Ye, C. Zhan, J. Hou, S. Zhang, B. Jiang, Y. Zhao, J. Huang, S. Zhang, Y. Liu, Q. Shi, Y. Liu, J. Yao, *Adv. Mater.* **2013**, *25*, 5791.
[38] Y.-J. Hwang, G. Ren, N. M. Murari, S. A. Jenekhe, *Macromolecules* **2012**, *45*, 9056.
[39] Y.-J. Hwang, T. Earmme, S. Subramaniyan, S. A. Jenekhe, *Chem. Commun.* **2014**, *50*, 10801.
[40] T. Earmme, Y.-J. Hwang, S. Subramaniyan, S. A. Jenekhe, *Adv. Mater.* **2014**, *26*, 6080.
[41] T. Earmme, Y.-J. Hwang, N. M. Murari, S. Subramaniyan, S. A. Jenekhe, *J. Am. Chem. Soc.* **2013**, *135*, 14960.
[42] N. Zhou, H. Lin, S. J. Lou, X. Yu, P. Guo, E. F. Manley, S. Loser, P. Hartnett, H. Huang, M. R. Wasielewski, L. X. Chen, R. P. H. Chang, A. Facchetti, T. J. Marks, *Adv. Energy Mater.* **2014**, *4*, 1300785.
[43] Y. Zhou, T. Kurosawa, W. Ma, Y. Guo, L. Fang, K. Vandewal, Y. Diao, C. Wang, Q. Yan, J. Reinspach, J. Mei, A. L. Appleton, G. I. Koleilat, Y. Gao, S. C. B. Mannsfeld, A. Salleo, H. Ade, D. Zhao, Z. Bao, *Adv. Mater.* **2014**, *26*, 3767.
[44] E. Zhou, J. Cong, Q. Wei, K. Tajima, C. Yang, K. Hashimoto, *Angew. Chem Int. Ed.* **2011**, *50*, 2799.
[45] N. M. Murari, M. J. Crane, T. Earmme, Y.-J. Hwang, S. A. Jenekhe, *Appl. Phys. Lett.* **2014**, *104*, 223906.
[46] D. Mori, H. Benten, I. Okada, H. Ohkita, S. Ito, *Adv. Energy Mater.* **2014**, *4*, 1301006.
[47] E. Zhou, J. Cong, K. Hashimoto, K. Tajima, *Adv. Mater.* **2013**, *25*, 6991.
[48] C. Mu, P. Liu, W. Ma, K. Jiang, J. Zhao, K. Zhang, Z. Chen, Z. Wei, Y. Yi, J. Wang, S. Yang, F. Huang, A. Facchetti, H. Ade, H. Yan, *Adv. Mater.* **2014**, *26*, 7224.
[49] E. Ahmed, T. Earmme, G. Ren, S. A. Jenekhe, *Chem. Mater.* **2010**, *22*, 5786.
[50] C. J. Tonzola, M. M. Alam, W. Kaminsky, S. A. Jenekhe, *J. Am. Chem. Soc.* **2003**, *125*, 13548.
[51] A. K. Agrawal, S. A. Jenekhe, *Chem. Mater.* **1996**, *8*, 579.
[52] A. K. Agrawal, S. A. Jenekhe, *Macromolecules* **1993**, *26*, 895.
[53] A. K. Agrawal, S. A. Jenekhe, *Macromolecules* **1991**, *24*, 6806.
[54] S. Subramaniyan, H. Xin, F. S. Kim, S. Shoaee, J. R. Durrant, S. A. Jenekhe, *Adv. Energy Mater.* **2011**, *1*, 854.
[55] H. Xin, S. Subramaniyan, T.-W. Kwon, S. Shoaee, J. R. Durrant, S. A. Jenekhe, *Chem. Mater.* **2012**, *24*, 1995.
[56] S.-H. Liao, H.-J. Jhuo, Y.-S. Cheng, S.-A. Chen, *Adv. Mater.* **2013**, *25*, 4766.
[57] S. Zhang, L. Ye, W. Zhao, D. Liu, H. Yao, J. Hou, *Macromolecules* **2014**, *47*, 4653.
[58] L. Ye, S. Zhang, W. Zhao, H. Yao, J. Hou, *Chem. Mater.* **2014**, *26*, 3603.
[59] C. Cui, W.-Y. Wong, Y. Li, *Energy Environ. Sci.* **2014**, *7*, 2276.
[60] Y. Liang, Z. Xu, J. Xia, S.-T. Tsai, Y. Wu, G. Li, C. Ray, L. Yu, *Adv. Mater.* **2010**, *22*, E135.
[61] T. Liu, A. Troisi, *Adv. Mater.* **2013**, *25*, 1038.
[62] H. Xin, X. Guo, G. Ren, M. D. Watson, S. A. Jenekhe, *Adv. Energy Mater.* **2012**, *2*, 575.
[63] J. K. Lee, W. L. Ma, C. J. Brabec, J. Yuen, J. S. Moon, J. Y. Kim, K. Lee, G. C. Bazan, A. J. Heeger, *J. Am. Chem. Soc.* **2008**, *130*, 3619.
[64] X. Guo, N. Zhou, S. J. Lou, J. Smith, D. B. Tice, J. W. Hennek, R. P. Ortiz, J. T. L. Navarrete, S. Li, J. Strzalka, L. X. Chen, R. P. H. Chang, A. Facchetti, T. J. Marks, *Nat. Photonics* **2013**, *7*, 825.
[65] J. D. Servaites, M. A. Ratner, T. J. Marks, *Energy Environ. Sci.* **2011**, *4*, 4410.
[66] Y. Zhou, C. Fuentes-Hernandez, J. Shim, J. Meyer, A. J. Giordano, H. Li, P. Winget, T. Papadopoulos, H. Cheun, J. Kim, M. Fenoll, A. Dindar, W. Haske, E. Najafabadi, T. M. Khan, H. Sojoudi, S. Barlow, S. Graham, J.-L. Brédas, S. R. Marder, A. Kahn, B. Kippelen, *Science* **2012**, *336*, 327.
[67] P. N. Murgatroyd, *J. Phys. D: Appl. Phys.* **1970**, *3*, 1488.

